THE EFFECT OF GAZE CONTINGENCY ON MULTIFOCAL ELECTRORETINOGRAMS

A thesis presented to the graduate faculty of New England College of Optometry in partial fulfillment of the requirements for the degree of Master of Science.

Alison Taylor

May 2024

© Alison Taylor

All Rights Reserved

The author hereby grants New England College of Optometry permission to reproduce and to distribute publicly paper and electronic copies of the thesis document in whole or in part.

DocuSign Envelope ID: ACFE9BCA-2248-4D46-8563-AC1560129AC1

THE EFFECT OF GAZE CONTINGENCY ON MULTIFOCAL ELECTRORETINOGRAMS

Alison Taylor

This manuscript has been read and accepted by the Thesis Committee in satisfaction of the thesis requirement for the degree of Master of Science

5/14/2024
Date

DocuSigned by:
78A8AD972399447...
Thanasis Panorgias, MS, PhD
Graduate Faculty Advisor

DocuSigned by:
41B8809FEE92419...
Alexis Malkin, OD, FAAO
Thesis Committee Member

DocuSigned by:
Fuensanta Vera-Diaz
1502BB240B7D484...
Fuensanta Vera-Diaz, OD, PhD, FAAO
Thesis Committee Member

DocuSigned by:
Anne Fulton
BAFAF099E5A94A6...
Anne Fulton, MD
Thesis Committee Member

5/14/2024
Date

DocuSigned by:
78A8AD972399447...
Thanasis Panorgias, MS, PhD
Director of Graduate Studies

ABSTRACT

The Effect of Gaze Contingency on Multifocal Electroretinograms

Alison Taylor

New England College of Optometry, 2024

PURPOSE: The objective of this study was to determine if the addition of gaze contingency to a multifocal electroretinogram (mfERG) stimulus had a significant effect on signal quality, the extent of eye movements, or the N1 and P1 signal components in subjects with normal vision. The ultimate goal is for this system to be used in subjects with fixation instability to improve the spatial specificity of mfERGs.

METHODS: A custom-built mfERG system was utilized both with and without gaze contingency, named the “GC” and “Fixed” conditions respectively. Recordings were successfully taken and analyzed from 8 subjects, each of which was tested in both conditions in a randomized order for comparison. The mfERG stimulus consisted of a 15x15˚ grid of 9 squares following a pseudorandom m-sequence. A signal-to-noise ratio (SNR) for each stimulus square was calculated to assess signal quality. Eye movements throughout testing were quantified using a bivariate contour ellipse area (BCEA) and kernel density estimation analysis (KDEA). The signals were further assessed by the N1 and P1 amplitude and implicit times.

RESULTS: The mean age of the 8 subjects used in the analysis was 24.63 ± 2.20 years (mean ± SD). When comparing the GC and Fixed conditions, there was no significant difference in SNR or eye movements ($p > 0.05$). It was determined that when all stimulus squares were taken into consideration, the GC condition had a significantly lower P1 amplitude and significantly longer P1 implicit time ($p<0.05$). When the stimulus was further separated into the central and peripheral squares, the peripheral squares had identical findings to those previously mentioned, while the central squares showed no significant differences between the two conditions.

CONCLUSIONS: With confirmation that the GC condition did not have an impact on SNR or eye movements compared to the Fixed condition, we can conclude the addition of gaze contingency did not negatively affect the signal response nor the subject's fixation. The differences in P1 amplitude may be explained by the correction of small eye movements in the GC condition, leading to increased spatial specificity and less crossover between high and low response areas on the retina. However, the differences in signal components also could have been a result of a system itself. Both of these explanations should be considered going forward in the use of this system.

ACKNOWLEDGEMENTS

I would first like to thank my advisor, Dr. Thanasis Panorgias, for his mentorship throughout the duration of my thesis. I am beyond grateful for his guidance, knowledge, and patience. I would also like to thank Dr. Sara Aghajari for her invaluable work creating the custom-built system in which this thesis is based on and for her support throughout the experimental process. Thank you to my thesis committee, Dr. Alexis Malkin, Dr. Fuensanta Vera-Diaz, and Dr. Anne Fulton, for their time and expertise in reviewing my thesis. Lastly, I thank my NECO peers, friends, and family for their support and encouragement.

TABLE OF CONTENTS

1. Introduction....1

1.1. The retina....1

1.1.1. Retinal anatomy....1

1.1.2. Imaging techniques....3

1.1.3. Functional testing....4

1.2. Multifocal electroretinogram....5

1.2.1. Background....5

1.2.2. Current applications....7

1.3. Fixation instability....8

1.3.1. The effects of eye movements on multifocal electroretinograms....8

1.3.2. Fixational eye movements....9

1.3.3. Gaze contingency....11

2. Rationale....12

3. Methods....13

3.1. Setting....13

3.2. Inclusion and exclusion criteria....13

3.3. Preliminary testing and preparation....14

3.4. Custom-built multifocal electroretinogram....15

3.4.1. Hardware....15

3.4.2. Hardware-software interface....16

3.4.3. Stimulus..... 16
3.5. Experimental design.....17
3.6. Analysis.....18
3.6.1. Signal-to-noise ratio.....18
3.6.2. Eye movements.....19
3.6.3. Signal components.....20
3.6.4. Statistical tests.....20
4. Results.....21
4.1. Subject characteristics.....21
4.2. Signal-to-noise ratio.....22
4.3. Eye movements.....24
4.4. Signal components.....27
5. DISCUSSION.....34
5.1. Signal-to-noise ratio.....34
5.2. Eye movements.....34
5.3. Signal components.....35
5.4. Correcting for multiple comparisons..... 40
5.5. General limitations.....40
5.6. Future applications.....41
6. Conclusions.....43
7. Bibliography..... 44

LIST OF FIGURES AND TABLES

Figure 1. Standard multifocal stimuli..... 6

Figure 2. Sample mfERG signal..... 6

Figure 3. Cone density map..... 9

Figure 4. Representation of mfERG stimulus conditions..... 18

Figure 5. Signal-to-noise ratio samples..... 23

Figure 6. Raw eye movement data samples..... 25

Figure 7. Quantification of fixation samples..... 26

Figure 8. Signals from each stimulus square in a recording..... 29

Figure 9. Bland-Altman Plots for All Stimulus Squares..... 30

Figure 10. Bland-Altman Plots for Central Stimulus Squares..... 31

Figure 11. Bland-Altman Plots for Peripheral Stimulus Squares..... 32

Figure 12. Cellular contributions to an mfERG..... 37

Figure 13. Photoreceptor and bipolar cell density in a primate retina..... 39

Table 1. Subject characteristics..... 21

Table 2. Quantification of fixation..... 24

Table 3. Significance testing..... 33

1. INTRODUCTION

1.1 THE RETINA

1.1.1 RETINAL ANATOMY

Prior to discussing the multifocal electroretinogram, it is first important to establish an understanding of the retina and how it can be assessed. The retina is a photosensitive tissue responsible for initiating and propagating the biochemical reaction that allows us to perceive visual stimuli. The retina consists of 10 histological layers with a complex and interconnected cellular structure that aids in visual processing. Functionally the retina is categorized into the retinal pigment epithelium and the neurosensory retina. The retinal pigment epithelium is a single layer responsible for nutrient transport and recycling waste products from the outer retina. The remaining 9 layers that form the neurosensory retina are responsible for signal transduction and consist of a photoreceptor layer, external limiting membrane, outer nuclear layer, outer plexiform layer, inner nuclear layer, inner plexiform layer, ganglion cell layer, nerve fiber layer, and internal limiting membrane[1].

For the purpose of this paper, it is most important to understand the function and composition of the photoreceptor layer, outer nuclear layer, outer plexiform layer, and inner nuclear layer. The photoreceptor layer consists of the outer segments of photoreceptor cells, which are responsible for converting light energy to a physiological signal called phototransduction. The outer nuclear layer is made up of the cell bodies of the rod and cone photoreceptors. The human retina contains four different photoreceptors, one rod and three cones, all of which contain different photopigments that determine its light absorption peak and spectrum. Rods predominate under scotopic conditions, while cones predominate in

photopic conditions and contribute to color vision and high spatial resolution. Synapses between photoreceptors and neighboring interneurons form the outer plexiform layer. The cell bodies of these interneurons lie in the inner nuclear layer and consist primarily of bipolar cells, which serve as a point of convergence for signal transmission of photoreceptor cells and help with visual processing[2].

Although the majority of the retina has a similar histological appearance, the unique specialization of the macula during development is responsible for our photopic visual performance. The macula is a 5-6 mm area in the central retina with a unique distribution of photoreceptor cell density. More peripheral areas of the macula serve as a transition point from a rod-dominated to cone-dominated retina, while the central most area, the fovea, has a notable change in appearance and composition. The fovea has a sloping characteristic in which the retina changes from having all distinct retinal layers to almost exclusively cones[3]. According to Curcio et al, the peak foveal cone density averages about 199,000 cones per mm^2, but has a considerable amount of variability between individuals[4]. This is dramatically higher than anywhere else in the retina. Another important but less obvious characteristic of the macula is the presence of "private lines". Typically, there is a convergence of multiple cones to a single OFF-bipolar cell (hyperpolarizing) or ON-bipolar cell (depolarizing), whereas private lines represent a 1:1 ratio[3]. The combination of these features is what provides humans with the potential for high visual acuity.

1.1.2 IMAGING TECHNIQUES

In clinical and academic settings, the retina can be visualized using different imaging modalities. Fundus photography has been used since the late 1800s to visualize the retina en face in live patients. Scanning laser ophthalmoscopy (SLO) is another imaging method that was invented in the 1980s and uses a single point of laser light to illuminate the retina as opposed to a bright flash as in fundus photography. This technique allows for reduced light scatter and therefore increased contrast. It can also be paired with a confocal apparatus providing selective images from a specific plane of the retina and can be used to construct a 3-dimensional fundus image. Another technique that can be incorporated is adaptive optics. Adaptive optics is a form of wavefront sensing that can measure and compensate for astigmatic and higher order aberrations. When this technology is paired with a fundus camera or SLO, it serves as a noninvasive method of producing images at a cellular level. Fundus autofluorescence (FAF) is another technique that can be used with standard imaging practices to highlight lipofuscin, a photoreceptor byproduct, by taking advantage of its fluorescent properties when excited by a specific wavelength. Optical coherence tomography (OCT) is arguably one of the most important clinical tools we have today to aid in retinal evaluation and diagnosis. OCT imaging provides a high resolution and cross sectional view of the retina by comparing reflected light waves from a reference path[5]. Although all of these imaging modalities serve as useful clinical tools, they provide only structural information instead of retinal function, which may precede structural changes.

1.1.3 FUNCTIONAL TESTING

The electro-oculogram (EOG) and electroretinogram (ERG) are two functional tests for assessing the retina, meaning they can be used to detect changes that may not be visible using currently available imaging methods. EOGs measure the change in voltage potential across the eye brought on by the polarization of the retinal pigment epithelium. Therefore, the EOG serves as a specific measure of assessing retinal pigment epithelial function[6]. On the contrary, the ERG assesses the function of the neurosensory retina using a light stimulus. Since the discovery of the ERG in 1865, its clinical use has been standardized into three different methods: full-field flash electroretinography (ffERG), pattern electroretinography (pERG), and multifocal electroretinography (mfERG)[7].

The ffERG distributes a diffuse series of flashes illuminating the entire retina simultaneously. The ffERG can be used to test the photopic and scotopic systems, for which the subject will be either light or dark adapted. Different stimulus variables, like luminances and flash intervals, can also be used to elicit various responses[8]. The main components of the ffERG recording are the a-wave, a negative deflection corresponding to photoreceptor function, and the b-wave, a positive deflection representing bipolar cell function[7]. Due to the nature of the stimulus of the ffERG, the values obtained provide a gross retinal response and is most appropriately used in conditions that diffusely affect the retina[8]. The pERG, unlike the ffERG, utilizes a reversing black and white checkerboard stimulus and targets only the macular region of the fundus. It is primarily used to record the function of cone-driven retinal ganglion cells. Although the retinal area stimulated in the pERG is much more localized than the ffERG, it too provides only a summed response[9]. The mfERG overcomes this limitation.

1.2 MULTIFOCAL ELECTRORETINOGRAMS

1.2.1 BACKGROUND

The mfERG was developed in 1992 by Sutter and Tran and is capable of simultaneously measuring the electrical activity of numerous distinct areas in the central retina opposed to a broad sum as demonstrated with other ERGs[10]. The spatial resolution of the mfERG is determined by the multifocal stimulus. In a standard mfERG, the stimulus consists of either 61 or 103 scaled hexagons, as shown in *Figure 1*, following a pseudorandom binary m-sequence[11]. The m-sequence is the series in which each hexagon displays one of two values, 0 or 1, with 0 representing a dark state (no luminance) and 1 representing a bright state (high luminance). As the hexagons follow this m-sequence, they appear to be flashing randomly and independently from each other. The retinal signal that is recorded as a response to the multifocal stimulation can then be cross-correlated with the m-sequence allowing for signal extraction that accurately represents the signal elicited by each individual hexagon[12]. The electrical signal acquired with the mfERG technique creates a waveform with a distinct negative deflection followed by a larger positive one. These are labeled as N1 and P1, respectively, as displayed in *Figure 2.* These waves are typically interpreted in measures of amplitude (electrical response) and implicit time (time of peak response from stimulus onset). In standard practice, emphasis is placed on analyzing N1 and P1 amplitude as well as P1 implicit time. The N1 amplitude is measured from baseline to the N1 trough, while P1 amplitude is measured from the N1 trough to P1 peak[11]. It has been shown that the cellular contributions of N1 are primarily OFF-bipolar cells and cones, while

the P1 is mainly ON-bipolar cells[13]. Cone responses predominate the mfERG due to the stimulus location, absence of dark adaptation, and temporal rate of stimulation[14].

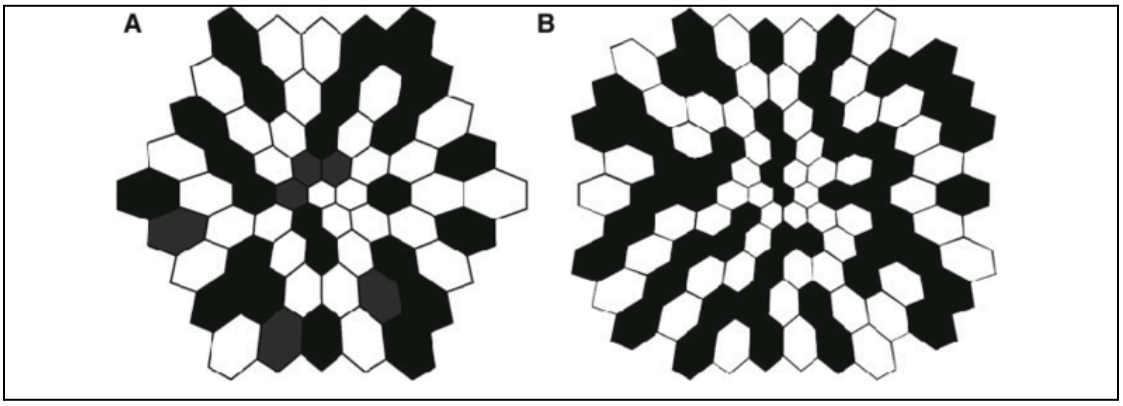


Figure 1) Standard multifocal stimuli. These diagrams adapted from Hood et al's "ISCEV standard for clinical multifocal electroretinography (mfERG) (2021 edition)" show samples of a 61 hexagon (A) and 103 hexagon (B) stimulus with scaled hexagons increasing in size with greater retinal eccentricity. These stimuli typically extend 40-50˚ of the visual field.[11]

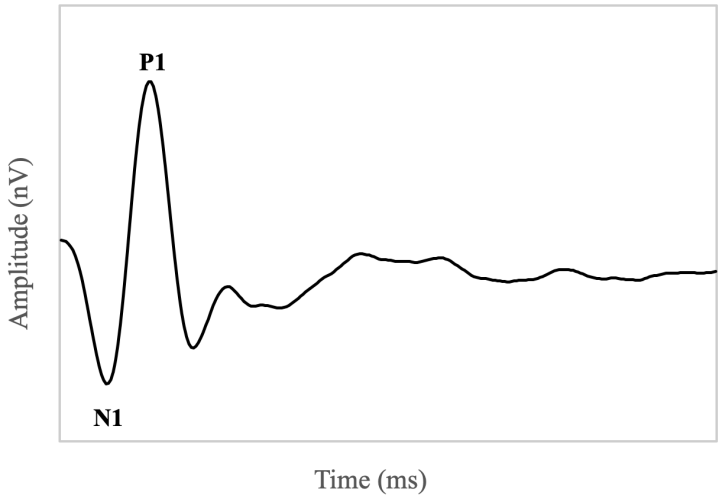


Figure 2) Sample mfERG signal. The trace above shows the N1 and P1 waves obtained from an mfERG recording.

1.2.2 CURRENT APPLICATIONS

MfERGs can be applied clinically as a sensitive measure of retinal function.[1]. When compared to the applications of the ffERG, the mfERG is most useful to assess conditions that affect the macula and posterior pole[15]. A topographical display of responses can be advantageous for visual field comparison, including blind spot mapping and scotoma detection[14]. MfERGs can also be used to aid in the evaluation of cases with unexplained vision loss[16] and as a diagnostic tool for retinal pathology and tracking disease progression[14]. Studies have been done using mfERGs on a wide variety of diseases that affect retinal structure and function.

One of the most prevalent diseases affecting the outer retina is age related macular degeneration (ARMD). ARMD has a multifaceted pathogenesis and is influenced by genetic and environmental risk factors[17]. In the dry (non-neovascular) form, the condition results in outer retinal deposits leading to clinical manifestations such as drusen, pigmentary changes, and geographic atrophy[18]. Research shows that subjects with ARMD of varying stages have reduced N1 and P1 amplitudes as well as delayed implicit times[19, 20].

Stargardt disease is a juvenile hereditary macular disorder that inhibits proper transport of phototransduction byproducts, ultimately leading to an accumulation of lipofuscin in the retinal pigment epithelium. Studies have shown that in patients with Stargardt disease there is a reduction in P1 amplitude and increased P1 implicit time[21, 22].

Another hereditary disorder that has utilized mfERG in clinical investigations is retinitis pigmentosa. Retinitis pigmentosa is a group of outer retinal disorders with similar characteristics that causes progressive visual field loss and ultimately affects central vision

later in life. Although studies have found consistent decreased mfERG response (P1-N1) in advanced cases, P1 implicit times are known to be variable[23].

1.3 FIXATION INSTABILITY

1.3.1 EFFECTS OF EYE MOVEMENTS ON MULTIFOCAL ELECTRORETINOGRAMS

Although the mfERG can be a useful tool in managing central retinal pathology, the spatial specificity of this test requires steady fixation. In healthy eyes, the response amplitude for a given area on the retina depends on eccentricity[24]. The fovea is expected to have the highest amplitude with a decreasing trend toward the periphery, mimicking the cone photoreceptor and bipolar cell distribution throughout the retina[24]. *Figure 3* from Curcio et al shows a cone density map of the fovea allowing for the visualization of how the number of cones in an individual changes as a function of retinal eccentricity. When fixation is lost, there may be crossover between these high and low density areas causing inaccurate representations of electrical activity. Similarly, people affected by macular disease may have a varied distribution of retinal function and are dependent on the spatial specificity of an mfERG to define and assess these areas.

Studies have been done demonstrating the effects that eye movements have on mfERGs. It has been shown that in normal subjects with simulated fixation instability, eye movements within the central stimulus hexagon (2.4˚) do not significantly affect the N1 or P1 amplitudes. However, the effect changes with larger magnitudes of fixation loss[25, 26]. Additionally, one study testing subjects with neovascular AMD found a negative correlation between the area of fixation and mfERG P1 amplitude within the central 5.6˚ of the

stimulus[26]. Fixation instability in Stargardt disease has also been shown to cause significantly lower test-retest reliability when compared to subjects with normal vision[27].

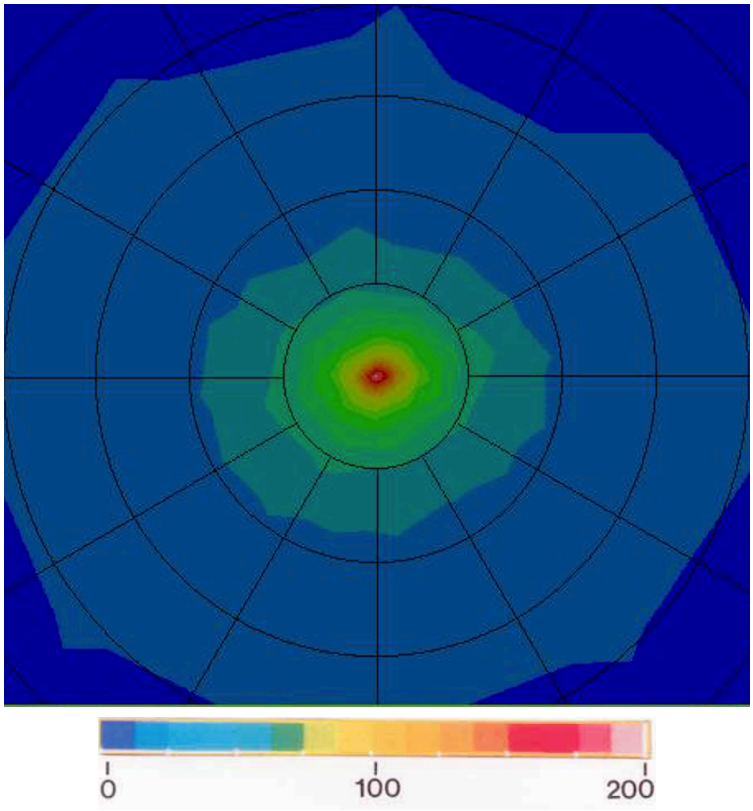


Figure 3) Cone density map. This figure adapted from Curcio et al's "Human Photoreceptor Topography" displays how the cone density of the retina changes with eccentricity in the fovea. The color coded scale at the bottom shows lower density on the left (blue) and higher density on the right (red). The grid shows intervals of 0.4mm. The scale represents cells x 1000 per mm^2.[4]

1.3.2 FIXATIONAL EYE MOVEMENTS

Although fixation appears to be a stagnant process, everyone is subject to small, involuntary eye movements during normal fixation called fixational eye movements. These

eye movements can be separated into three distinct types; tremor, drifts, and microsaccades[28]. Tremor is a high frequency motion with the smallest amplitude extending on average one foveal cone diameter. Drift is a slow movement that occurs between microsaccades and may extend across a few dozen photoreceptors. Microsaccades are small jerk-like movements and are the largest of the three types with the potential to cross up to several hundred photoreceptors[29]. Of these fixational eye movements, microsaccades appear to be the most studied and well defined. Microsaccades are known to occur as a means of counteracting neural adaptation during fixation that would otherwise lead to perceptual blindness of stationary objects[28].

People with macular pathology are known to have significantly larger degrees of fixation instability compared to controls. One study found that when comparing fixational eye movements in these populations, those with macular disease exhibited larger amplitudes of drifts and microsaccades. Using a linear regression analysis, they were able to determine that the amplitude of microsaccades play a significant role in determining fixation instability[30].

According to current ISCEV standards, fixation should be monitored for all mfERG recordings using either direct observation or, more commonly, camera based technology to track the pupil or fundus. In the presence of significant eye movements, their recommendation is to discard contaminated segments and repeat the test. Blinks may also lead to distorted waveforms and should be treated similarly[11]. Although this solution does eliminate the inaccuracies attributed to fixation loss, this can result in excessive testing for

subjects. It also contributes to unnecessary subjectivity within the experiment, having to choose a subjective threshold of inadequacy.

1.3.3. GAZE CONTINGENCY

To mitigate the effect of fixational instability, several psychophysical studies have employed the technique of "gaze contingency." The term "gaze contingent" refers to the utilization of an eye-tracker that is used to update the location of a stimulus in real time such that it may project onto the same retinal location throughout testing. One study by Loschky and McConkie used a bi-resolutional, gaze contingent display consisting of a high resolution central window and low resolution periphery to assess eye movements and search times[31]. Another study by Ganesan et al used a gaze contingent central scotoma to test a new method of saccadic re-referencing to a peripheral retinal point[32]. Although both of these examples utilized gaze contingency, they simulated a scenario instead of serving a corrective purpose. One study demonstrating the latter by Dorr and Bex used a gaze contingent display to improve fixation in the assessment of contrast sensitivity under natural viewing conditions[33]. In this study, we used a custom-built gaze contingent mfERG system to resolve the problem introduced by fixational instability, as described above. In essence, the location of the mfERG stimulus on the screen was continuously updated to follow the subject's gaze, such that the stimulus was always projected on the same retinal location. To date, there is no other published research using this unique approach to correct fixation during mfERG testing. The ultimate goal of this system is to increase the spatial accuracy of mfERGs so as to obtain a more specific measure of retinal function.

2. RATIONALE

The purpose of the present study is to assess the effects of a gaze contingent stimulus on an mfERG in subjects with normal vision. The study will serve as a proof of concept to determine whether or not gaze contingency generates significant distortions in signal response or if a mobile display impacts the extent of a subject's eye movements when compared to a non-gaze contingent stimulus. Furthermore, the N1 and P1 amplitudes and implicit times will be assessed to determine if the correction of normal fixational eye movements have a significant impact on the acquired signal.

3. METHODS

3.1 SETTING

The study took place at New England College of Optometry in Boston, Massachusetts. All subjects were recruited from within the institution. Study details and contact information were distributed via email. A total of 11 subjects were tested with the custom-built mfERG system and stimulus detailed below. Additional subjects were recruited and tested using a different stimulus, but their data are not included in the present study due to technical limitations. Using an *a priori* power analysis based on a published study comparing the reproducibility of mfERGs using different instruments[34], it was determined that 10 subjects would be required to obtain a power of 0.9 for a significance level of 0.05.

3.2 INCLUSION AND EXCLUSION CRITERIA

Subjects between the ages of 18-65 years were eligible to participate in this study. Known ocular health was to be within normal limits and visual acuity had to be Snellen equivalent of 20/25 (0.1 logMAR) or better in the tested eye. Subjects were excluded from the study if they had a history of any systemic/neurological disease that might affect vision or the presence of any ocular disease, strabismus, or amblyopia. Due to the nature of the stimulus used in the experiment, subjects with a history of epilepsy or seizures were excluded. Subjects unable or unwilling to have their pupils dilated were also excluded from the study.

3.3 PRELIMINARY TESTING AND PREPARATION

The purpose and details of the experiment were explained to each subject prior to the beginning of the study. The session was estimated to take between 1.5 and 2 hours. The subject was asked to sign the consent form only after their questions had been answered to their satisfaction. The subjects then proceeded to complete a questionnaire confirming their demographics and health. The subject's ETDRS visual acuity was measured with their best correction and an autorefractor (Nidek, ARK-700A**)** was used to obtain an objective measurement of refractive error. Corrective lenses worn by the subject were read using a manual lensometer. The subject's intraocular pressure (IOP) was then measured using a non-contact tonometer (Topcon, CT-80**)** and the Van Herick technique was used to assess the anterior chamber depth**.** An IOP greater than 21mmHg and/or a Van Herick estimation smaller than ½:1 were considered unfit for dilation. If the subject fit the inclusion criteria, they were asked to continue with the experimental part of the study. If they were not able to proceed with testing, they were compensated for their time up until that point.

Subjects were then dilated with 0.5% tropicamide in one eye and recordings were obtained at least 20 minutes after instillation. If both eyes were eligible, the tested eye was randomly selected. If one eye was not eligible, the other eye was chosen. A DTL electrode and two skin electrodes were applied; one ground electrode and one reference electrode. Subjects were then fitted with a trial frame that contained their habitual prescription plus a +1.75D add in both eyes to account for the viewing distance between the monitor and the subject (54 cm). Subjects were positioned in front of the monitor using a chin and forehead rest for stability. An additional strap was placed around the back of the head for further head

stabilization to avoid movement throughout testing. Both eyes remained open for the duration of testing. If the subject experienced diplopia at any point throughout the experiment, the non-tested eye was to be occluded. Dim room lighting was used during mfERG data acquisition.

3.4 CUSTOM-BUILT MULTIFOCAL ELECTRORETINOGRAM

The development of the custom-built mfERG system is out of the scope of this thesis. Here we provide the technical details necessary for understanding the basic operation of the gaze-contingent mfERG system.

3.4.1 HARDWARE

The system consisted of a stimulus generator (Bits#, Cambridge Research Systems, UK) controlled by Matlab (Mathworks, MA, US) and the Psychtoolbox (Ref) extensions on a Linux PC. The stimulus was presented on an LCD monitor (LG, 120 Hz) in front of which a video-based eye-tracker (Eyelink 1000, SR Research, Canada, 2000 Hz sampling rate) was placed to record the subject's gaze. The physiological signal was recorded by a system consisted of a Grass 15LT Physiodata physiological amplifier (Grass Technologies, US, 100K gain, 10-100 Hz bandpass filter, 0.96KHz sampling rate), a Power1901 data acquisition system (DAQ) and the Signal 7 software for data storing and processing (Cambridge Electronic Design, UK). A photodiode was placed at the top left corner of the monitor recording the luminance changes corresponding to the central stimulus square in order to detect any dropped frames or artifacts in the stimulus presentation.

3.4.2 HARDWARE-SOFTWARE INTERFACE

The acquisition system was triggered by the BITS# stimulus generator to allow for a time-locked data collection. Each time the eye-tracker detected a blink it generated a trigger pulse that was recorded through the DAQ system to sync the event with the recorded physiological signal. When blinks were detected, the stimulus presentations 0.7 sec prior to the detection of the blink to 3 sec after the end of the blink was repeated to improve the signal quality. The eye's position was recorded with an analog signal generated by the eye tracker and recorded by the DAQ system. The eye-tracker that was continuously monitoring the subject's fixation was interfaced with the stimulus control PC so that the stimulus location on the screen could be updated according to the location of the subject's gaze. To ensure accuracy, the eye-tracker was calibrated to each individual subject prior to the start of each mfERG.

3.4.3 STIMULUS

The mfERG stimulus was a symmetric 3x3 grid of equally sized squares (9 squares total) extending 15x15˚ visual angle (5x5˚ per square). A fixation point was always present in the middle of the central square surrounded by a 2˚x2˚ red square outline. The red square outline was used to alert the subjects when their gaze was deviating too far from the center of the screen. When the subject's fixation was more than 2˚ away from the center of the screen, the red square changed its color to green to indicate to the subject that they need to fixate back to the center of the screen.

The nine squares were either black or white, following a pseudorandom binary m-sequence of 12 resulting in 2^{12}-1 states (4095 states). Each state consisted of two main frames (black or white) and four filler frames that were always black. Therefore, a state consisted of six frames with a duration of 50 ms (6x8.333 ms for 120 Hz). Therefore, an m-sequence of 12 would need 4095 x 50 ms or 204.74 seconds to complete a full cycle, which is the total duration of the multifocal recording. The recording was further divided into 11 recording segments each lasting approximately 18 seconds.

3.5 EXPERIMENTAL DESIGN

The system was used to test subjects under two conditions (see *Figure 4)*. In both conditions, the subjects were asked to fixate on the target in the center of the screen. In the standard or “Fixed” condition, the stimulus was stationary (fixed) on the screen. In the gaze-contingent or “GC” condition, the stimulus actively followed the subject's gaze throughout testing based on the positional data obtained by the eye tracker. The order of the two conditions was randomized for each subject. All experiments were actively being observed and monitored by the operator. If a subject had too many blink trigger signals during any given recording segment, it was immediately repeated and replaced. This was determined on an observational basis using the Signal 7 software when the recording of a particular segment was prolonged to more than 30 seconds. Although a full calibration of the eye-tracker was only done at the start of the mfERG in each condition, in-between recording segments there were brief re-calibrations to account for any minor head movements or positioning errors.

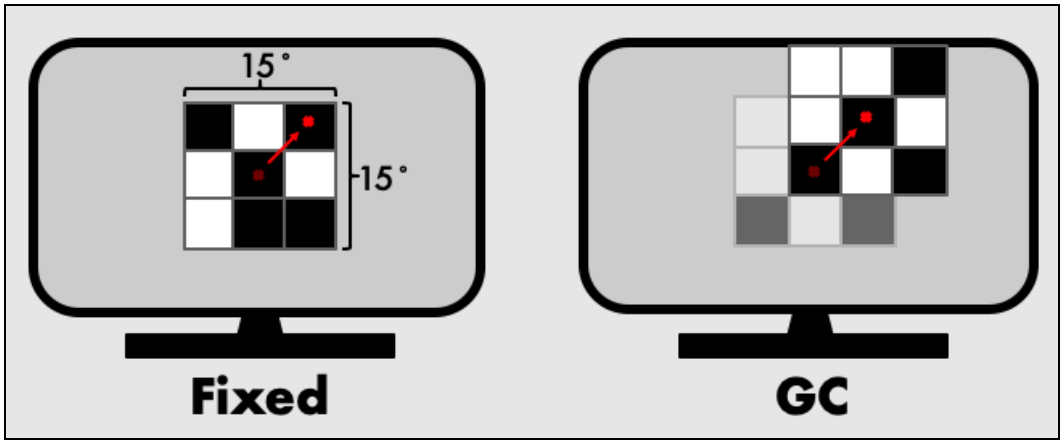


Figure 4) Representation of mfERG stimulus conditions. The figure above shows a simplistic diagram representing the difference between the two testing conditions. The Fixed condition on the left shows the stimulus pattern stationary on the screen in the setting of a change in fixation, indicated by the red squares. The GC condition on the right shows how the stimulus moves with a change in fixation.

3.6 ANALYSIS

3.6.1 SIGNAL-TO-NOISE RATIO

The signal-to-noise ratio (SNR) for each stimulus square was calculated to assess the quality of the recordings. The equations used for SNR calculations (*Equations 1-3*) were modeled after a paper from Zhang et al analyzing multifocal VEPs[35]. We calculated the SNR as the ratio between the Root-Mean Square (RMS) of the recording during a time window (1 to 81 ms) that contained the signal of interest, and a time window (196 to 277 ms) containing noise. Therefore, a good recording would consist of an RMS_{signal} that is high and an RMS_{noise} that is low, resulting in a high SNR.

Equations 1-3) Signal-to-noise ratio.

1. $SNR = RMS_{signal} / RMS_{noise}$

2. $$RMS_{signal} = \left[\sum_{i=1}^{81} (X_i - Mean_{1\text{-}81})^2 / N \right]^{1/2}$$

3. $$RMS_{noise} = \left[\sum_{i=196}^{277} (X_i - Mean_{196\text{-}277})^2 / N \right]^{1/2}$$

3.6.2 EYE MOVEMENTS

Eye movement data for each subject was analyzed using both the bivariate contour ellipse area (BCEA) method and the kernel density estimation analysis (KDEA). The BCEA is the standard method of assessing eye movements in normally distributed data. The area of an ellipse that includes 95% of the eye's locations is fitted and calculated using this method. The KDEA is a non-parametric means of analyzing the data. With this method, iso-probability density areas are calculated. A high KDEA value indicates that there is a high probability that the eye's location will fall within that certain area. In our case, we calculated the KDEA iso-probability density areas to include 95% of the data points. Although the mfERG data collected during blinks and out of range eye movements were re-recorded to improve the signal quality, all eye movements were to be included in this portion of the analysis, to highlight the extent of deviations from the fixation point during an mfERG recording.

3.6.3 SIGNAL COMPONENTS

The mfERG components used in this study were chosen according to ISCEV standards that include N1 and P1 amplitudes and implicit times. When comparing the two conditions, the differences were calculated by subtracting the Fixed condition from the GC condition (GC - Fixed). N1 values are expected to be negative, and therefore a negative difference of GC - Fixed indicates a larger relative response from the GC condition, while a positive difference is correlated to a larger relative response from the Fixed condition. P1 values are expected to be positive, therefore a positive difference of GC - Fixed indicates a larger relative response from the GC condition while a negative difference is correlated to a larger relative response from the Fixed condition. N1 and P1 implicit times with a positive difference indicate a shorter implicit time in the Fixed condition while a negative difference indicates a shorter implicit time in the GC condition.

3.6.4 STATISTICAL TESTS

When comparing the two different conditions, Fixed and GC, each data set was tested for normality. Depending on the sample size, the Kolmogorov-Smirnov test (samples >50) or the Shapiro-Wilk test (samples <50) was used to determine if the data was significantly different from a normal distribution. If both conditions were normally distributed, a paired t-test was then used to compare the data. If one or both of the conditions did significantly differ from normality, a non-parametric equivalent of the paired t-test was applied. For larger sample sizes, the data was compared using the Wilcoxon Signed-Rank test and for smaller sample sizes the Sign test was used. Significance was defined as a p value of less than 0.05.

4. RESULTS

4.1 SUBJECT CHARACTERISTICS

A total of 8 healthy subjects were included in the study. 11 subjects were formally recruited and compensated for their time and 10 subjects were able to complete testing. Of the 10 subjects that completed the experiment, the raw data from two additional subjects were unable to be analyzed due a computational error and were therefore excluded. For the 8 subjects included in the final analysis, their mean age was 24.63 ± 2.20 years (mean ± SD) with a range from 23 to 29 years. The average visual acuity in the test eye was -0.015 ± 0.035 logMAR (mean ± SD). Data was collected in the left eye of 6 subjects and the right eye of 2 subjects. All subjects included were able to complete testing binocularly. Additional subject information can be found in *Table 1*.

Table 1) Subject characteristics. The table below shows a record of subject data, displaying information from the questionnaire as well as visual parameters that were obtained as a part of the preliminary testing.

Subject	Age (years)	Gender	Ethnicity	Race	Test Eye	Visual Acuity (logMAR)	Refractive Error in Test Eye
1	23	F	Non-hispanic	Black	OS	0.0	-5.00 -0.50 x 015
2	23	F	Non-hispanic	White	OS	0.0	-0.25 -0.25 x 090
3	29	F	Non-hispanic	White	OS	-0.02	plano
4	23	F	Non-hispanic	White	OS	0.0	-1.75 -0.75 x 020
5	23	F	Non-hispanic	White	OS	0.0	plano
6	24	F	Non-hispanic	White	OS	0.0	-2.50 -0.50 x 090
7	26	F	Non-hispanic	Asian	OD	0.0	plano
8	23	F	Non-hispanic	White	OD	-0.1	-2.75 sphere

4.2 SIGNAL-TO-NOISE RATIO

After calculating the SNR across all stimulus squares in the 8 subjects, there was no statistically significant difference between the Fixed and GC conditions (*Wilcoxon Signed-Rank test, p* = 0.208, W = 1090). The average SNRs in the Fixed and GC conditions were 5.87 ± 3.18 and 5.57 ± 3.59 (mean ± SD), respectively. For the remainder of the analysis, signals with a SNR of less than 2.0 were excluded from the study. A threshold of 2.0 was established subjectively in an effort to balance the elimination of traces with too much noise while also not excluding potentially viable data. Examples of recordings with a high and low SNR can be seen in *Figure 5*. Only 4 squares of the total 144 analyzed were removed based on this criterion and all were from the same subject (subject 4). All 4 were from peripheral squares, 3 of which were from the GC condition and 1 from the Fixed condition. This resulted in the removal of 4 sets of stimulus squares from further analysis.

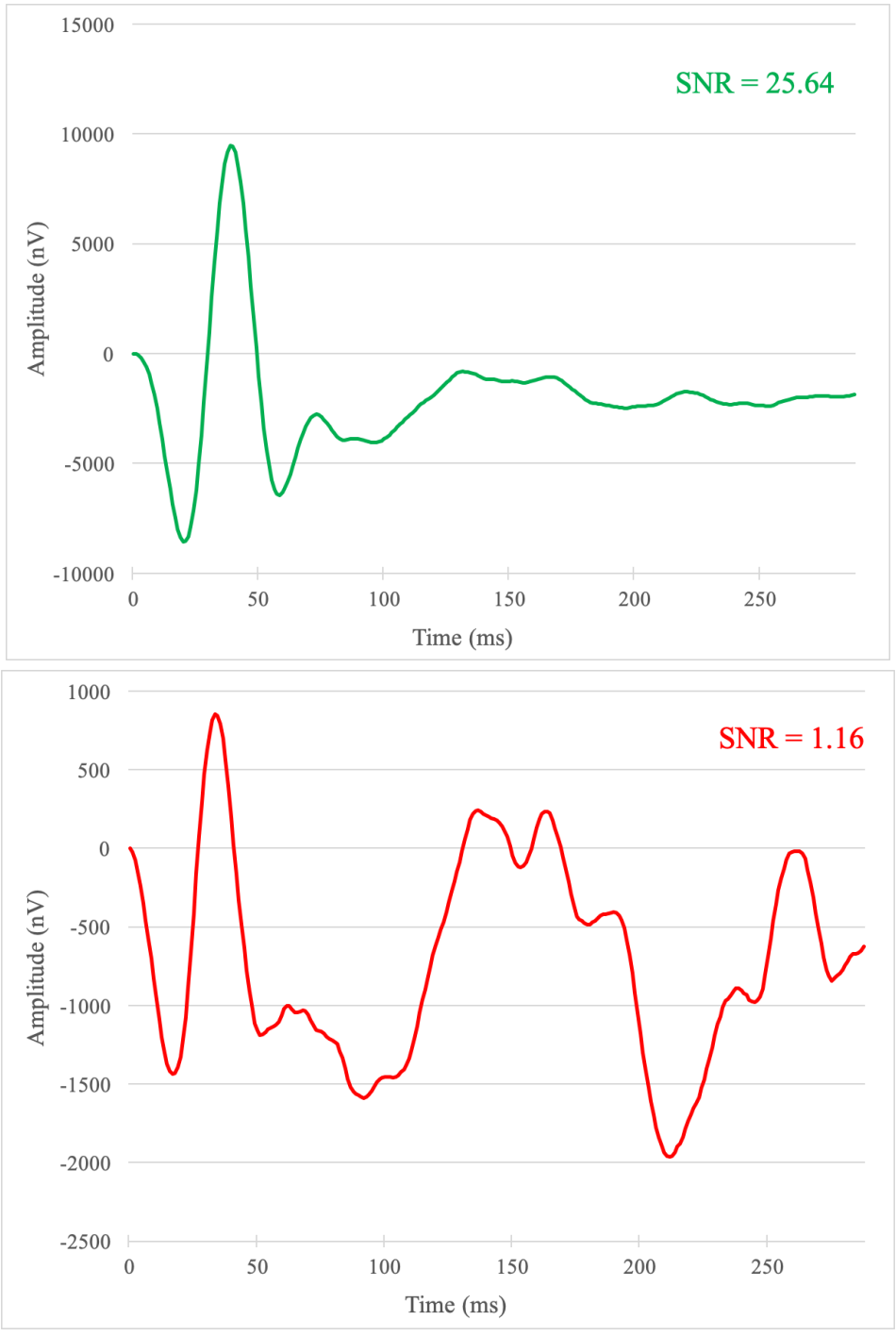


Figure 5) Signal-to-noise ratio samples. The figure above shows a sample trace of a central stimulus square that had the highest SNR (top panel) and a peripheral stimulus square that had the lowest SNR (bottom panel).

4.3 EYE MOVEMENTS

Using the BCEA, the average calculated area of eye movements was 3.14 ± 1.23 degrees^2 in the Fixed condition and 3.78 ± 1.83 degrees^2 (mean ± SD) in the GC condition. The difference between the two conditions was not statistically significant (*Sign test, p* = 0.479, *X* = 5). Using the KDEA, the average calculated area of eye movements was 2.55 ± 0.55 degrees^2 in the GC condition and 3.44 ± 2.11 degrees^2 (mean ± SD) in the Fixed condition. The difference between the two conditions was not statistically significant (*Sign test, p* = 1, *X* = 4). Although the eye movement data was not normally distributed, the BCEA is still presented in addition to the KDEA due to its familiarity in literature. Individual calculations for BCEA and KDEA are shown in *Table 2.* Samples of eye movement data from two subjects for the same stimulus condition are displayed in *Figure 6* and *Figure 7.*

Table 2) Quantification of fixation. The table below displays the areas of fixation as calculated by the BCEA and KDEA for each condition.

Subject	**BCEA (deg^2)**	**KDEA (deg^2)**	**BCEA (deg^2)**	**KDEA (deg^2)**
1	3.31	2.41	3.42	3.08
2	2.50	2.29	7.59	8.20
3	2.79	2.84	2.53	2.33
4	5.61	3.73	2.76	3.13
5	2.12	2.24	5.42	4.35
6	3.02	2.28	3.29	2.12
7	4.08	2.69	3.00	2.88
8	1.71	1.93	2.13	1.43
Mean ± SD	3.14 ± 1.23	2.55 ± 0.55	3.78 ± 1.83	3.44 ± 2.11

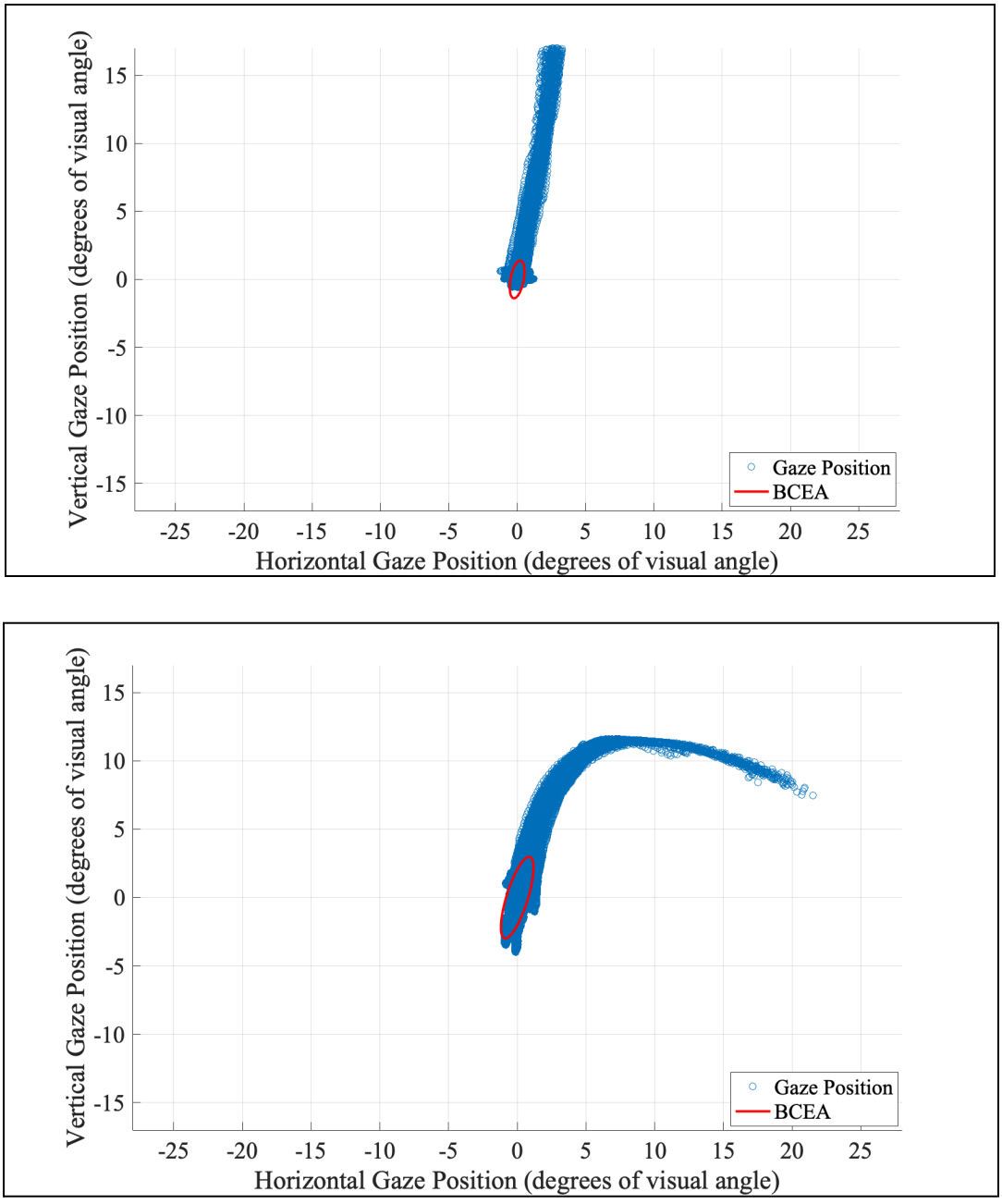
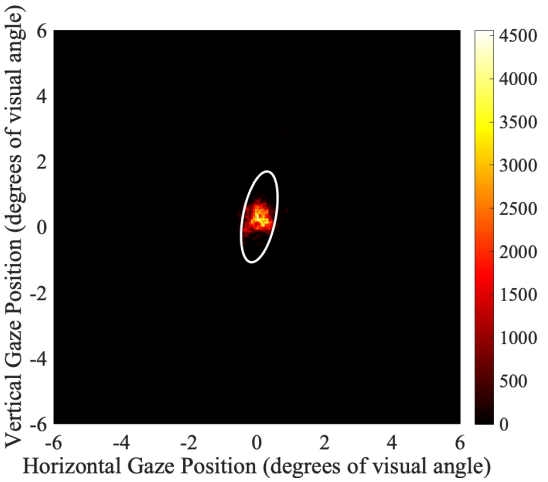
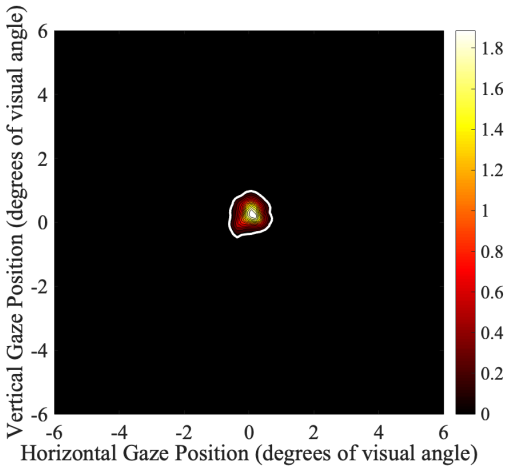


Figure 6) Raw eye movement data samples. The top panel displays all eye movements from a better fixator in one of the stimulus conditions, while the bottom displays that of a worse fixator in the same stimulus condition. The axes mimic the size of the display screen to demonstrate the full extent of the subject's eye movements. The location 0,0 corresponds to the central fixation point of the stimulus. The subjects and conditions shown here are the same as in Figure 7. The BCEA of the two subjects are also displayed and identical to that shown in Figure 7.

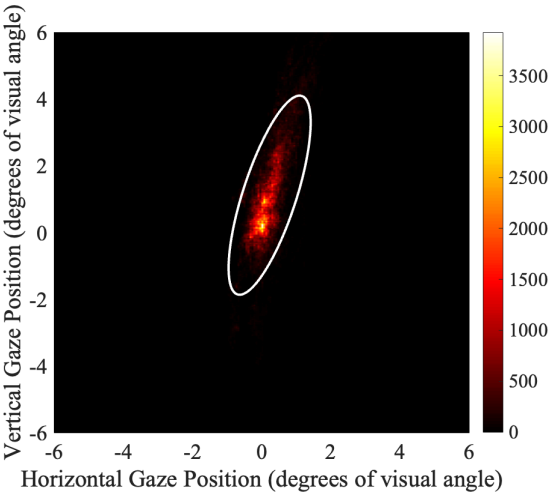
A) BCEA (top panel, Figure 6)



B) KDEA (top panel, Figure 6)



C) BCEA (bottom panel, Figure 6)



D) KDEA (bottom panel, Figure 6)

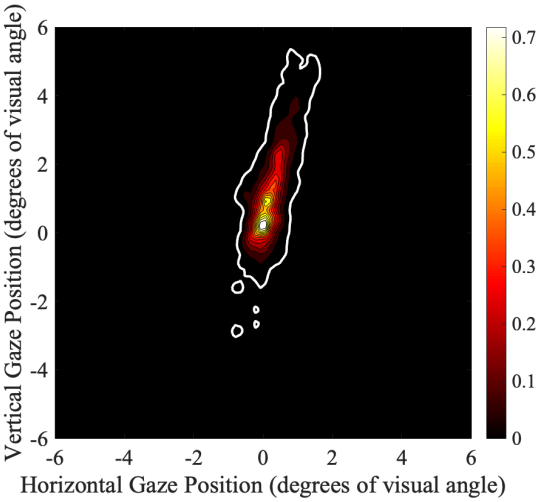


Figure 7) Quantification of eye movement samples. Samples of BCEA and KDEA are displayed above. The BCEA plots show the calculated ellipses that enclose 95% of the eye movement data. The KDEA plots show the calculated iso-probability density areas that correspond to the areas that 95% of the data will fall on. Using the colored scale, lighter colors indicate higher frequency of gaze location and darker colors indicate lower frequency of gaze location. The location 0,0 corresponds to the central fixation point of the stimulus. A and B serve as an example of better fixation and represent the same subject and condition as the top panel of Figure 6, compared to C and D which exhibit an example of worse fixation representing the same subject and condition as the bottom panel of Figure 6.

4.4 SIGNAL COMPONENTS

After removing the data corresponding to signals with an SNR lower than 2.0, the remaining data was analyzed for each signal component. The group average difference in N1 amplitude between the GC and Fixed conditions was +180.12 ± 938.85 nV (mean ± SD) and was not statistically significant (*Wilcoxon Signed-Rank test, p* = 0.112, W=913). The average difference in N1 implicit time between the two conditions was +0.29 ± 1.23 ms (mean ± SD) and was also not statistically significant (*paired t-test, p* = 0.056, t=1.948). For the P1 amplitude and implicit time, the average differences were found to be -413.64 ± 1176.04 nV and +0.49 ± 1.13 ms (mean ± SD), respectively. The GC condition resulted in a significantly lower amplitude (*paired t-test, p* = 0.005, t=2.900) and a significantly longer implicit time (*paired t-test, p* = 0.001, t=3.575) when compared to the Fixed condition.

After analyzing all of the stimulus squares together, the data was then re-analyzed separating the stimulus into two categories; the central square (1) and the peripheral squares (8). For the central square, the average difference for the N1 amplitude and implicit time were +181.48 ± 1125.07 nV and +0.13 ± 0.67 ms (mean ± SD), respectively. The average differences in P1 and implicit time were -829.24 ± 1759.40 nV and +0.26 ± 0.74 ms (mean ± SD), respectively. Using the appropriate tests based on the normality of the data, it was determined that none of the 4 components were significantly different between the two conditions for the central square (see additional details in *Table 3)*.

For the 8 peripheral squares, the average difference for the N1 amplitude was +179.94 ± 922.38 nV (mean ± SD) and was not statistically significant (*paired t-test*, *p* = 0.1361, t=1.511). Similarly, the average difference in N1 implicit time was also not

significant between the two conditions (*paired t-test, p* = 0.066, t=1.875) and had an average difference of +0.31 ± 1.29 ms (mean ± SD). However, when looking at the P1 data, the difference in amplitude and implicit time between the conditions were both significantly different. The average difference in amplitude was -358.14 ± 1084.76 nV (mean ± SD) (*paired t-test, p* = 0.013, t=2.557) and implicit time was +0.52 ± 1.17 ms (mean ± SD) (*paired t-test, p* = 0.001, t=3.435). This means that the signal amplitude elicited by the peripheral squares in the GC condition was significantly reduced and the implicit time was significantly longer when compared to the Fixed condition. The results for the peripheral squares mimic the initial results when all squares were used in the comparison.

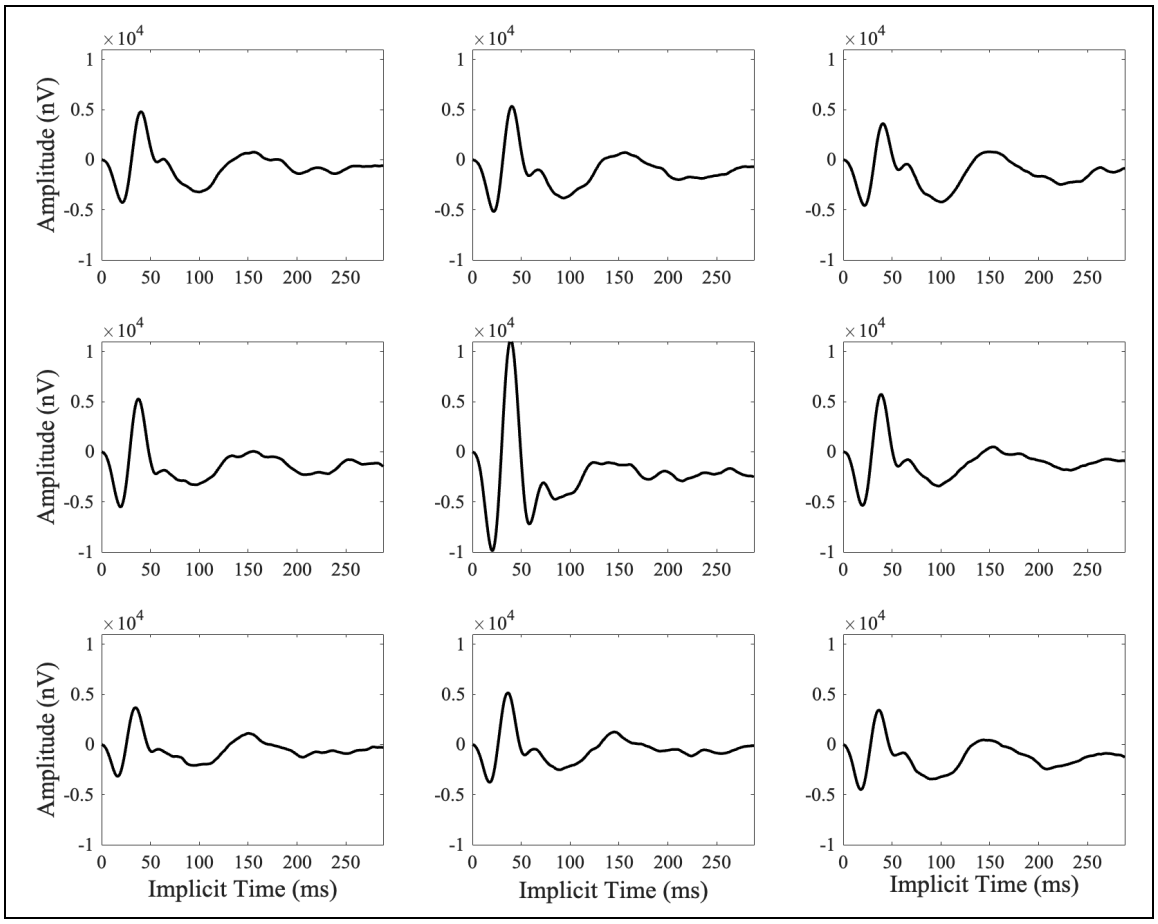
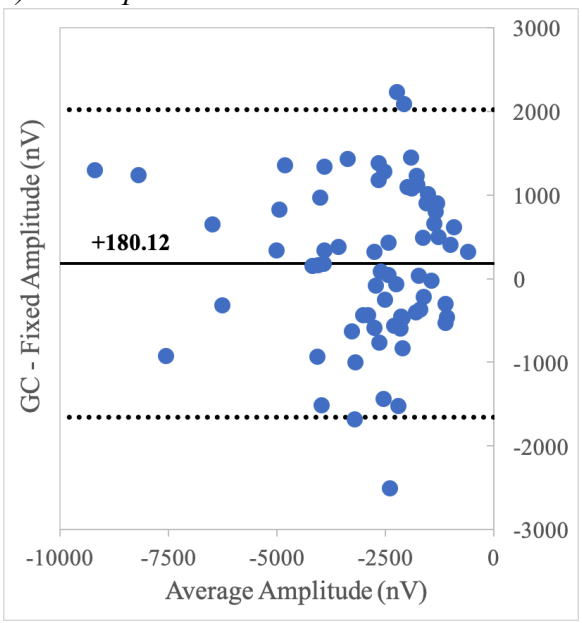
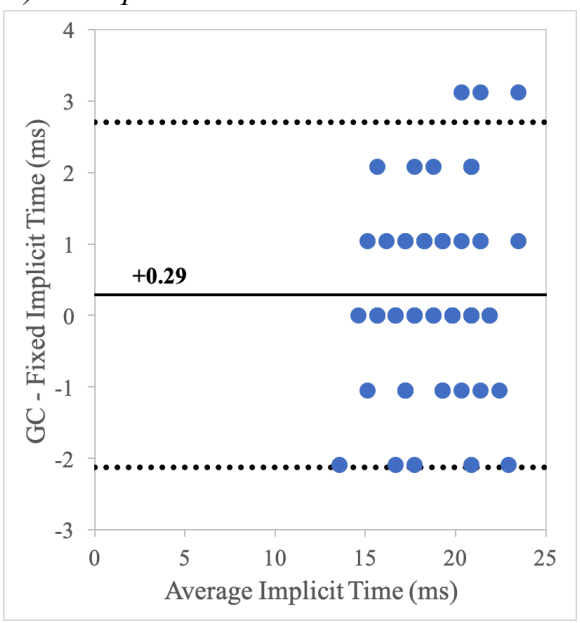


Figure 8) Sample signals from each stimulus square for one recording. The panel of traces corresponds to all of the signals obtained from a single subject for one of the stimulus conditions. The middle trace represents the central stimulus square and the remaining traces represent each peripheral square.

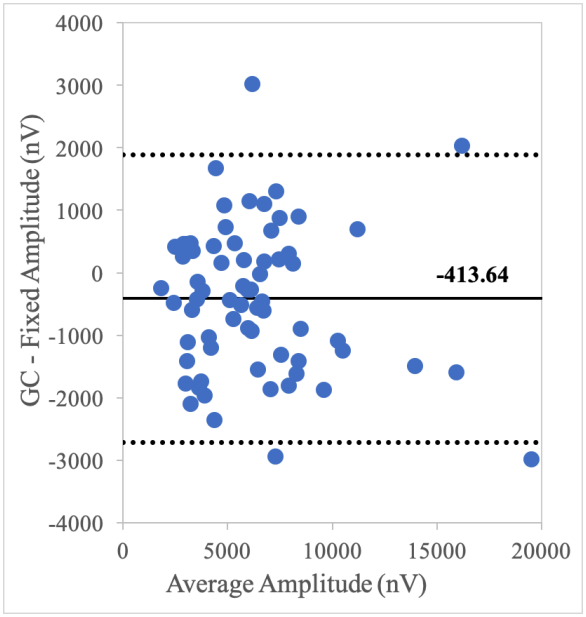
A) N1 Amplitude



B) N1 Implicit Time



*C) P1 Amplitude**



*D) P1 Implicit Time**

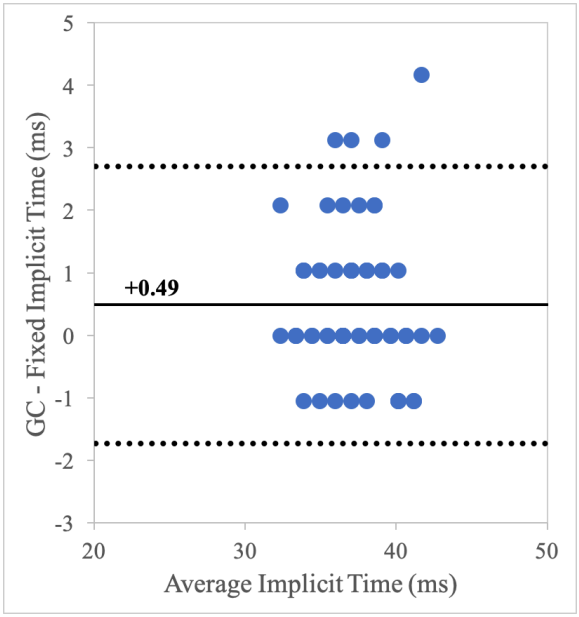
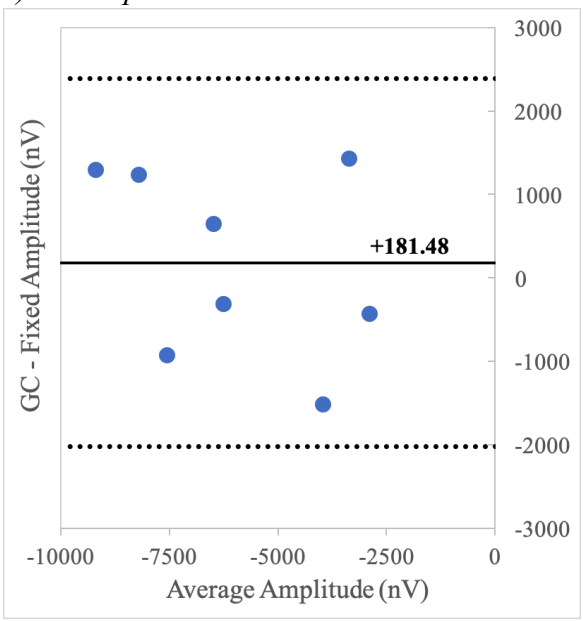
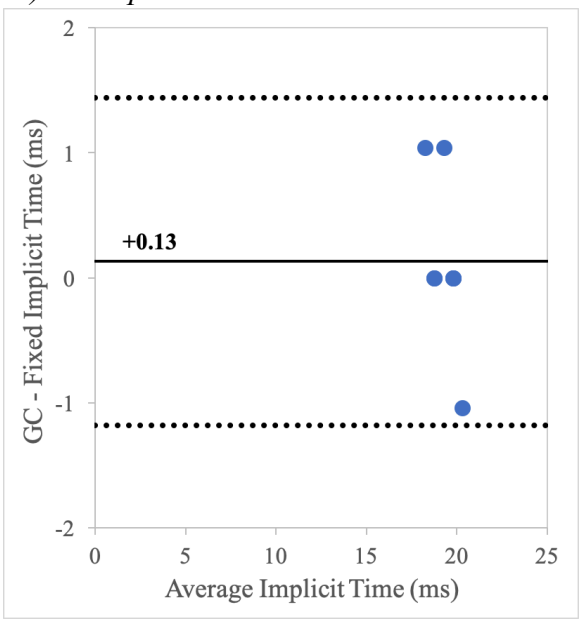


Figure 9) Bland-Altman Plots for All Stimulus Squares. The solid line represents the average difference between GC and Fixed conditions. The dotted lines represent the upper and lower limit of 95% confidence. Asterisks indicate components with a statistically significant difference between conditions. The linear appearance of the data points in the implicit time plots is due to the temporal resolution of the system (1.04 seconds).

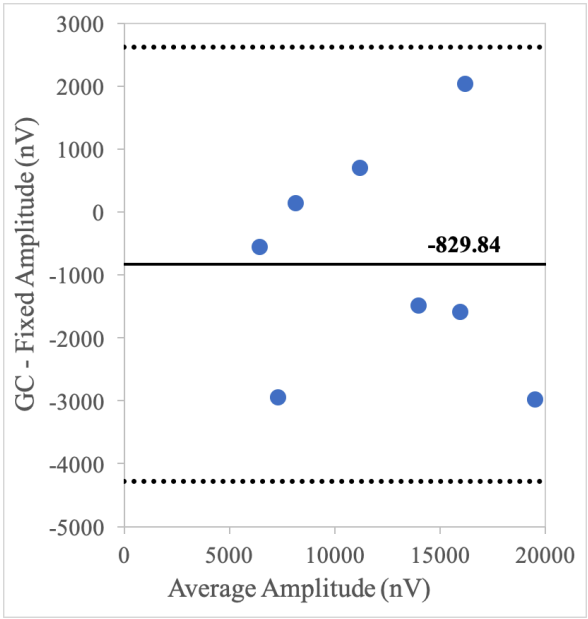
A) N1 Amplitude



B) N1 Implicit Time



C) P1 Amplitude



D) P1 Implicit Time

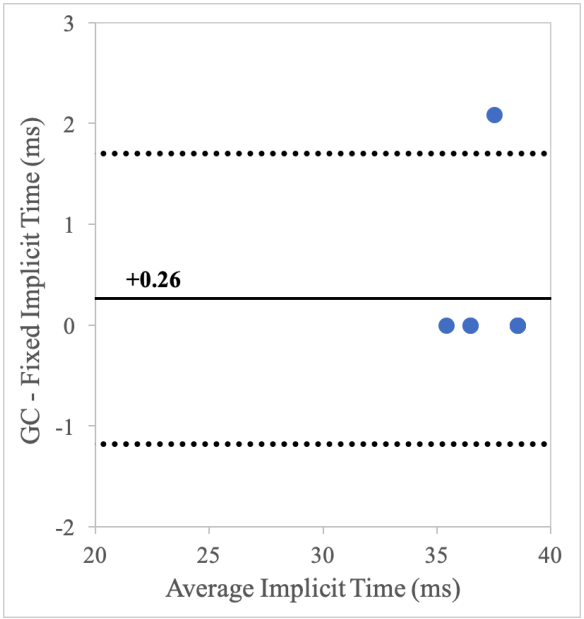
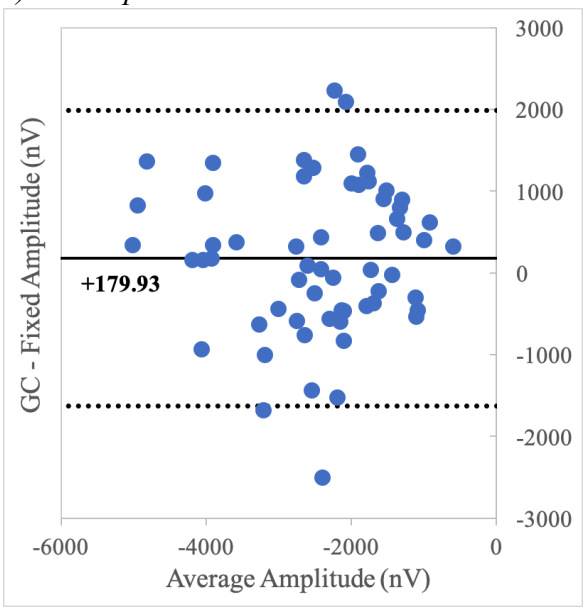
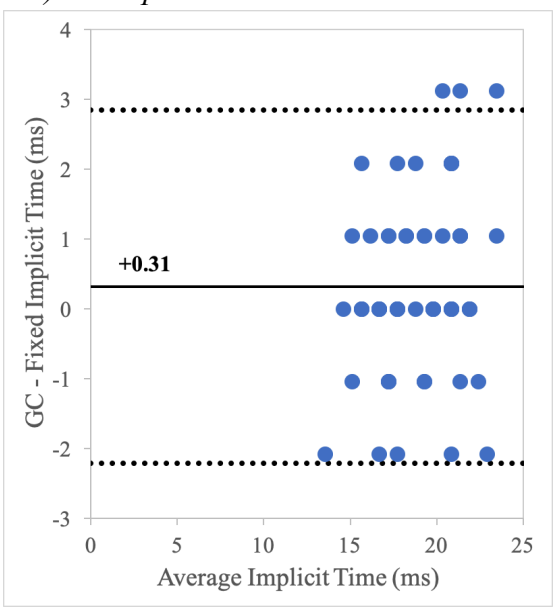


Figure 10) Bland-Altman Plots for Central Stimulus Squares. The solid line represents the average difference between GC and Fixed conditions. The dotted lines represent the upper and lower limit of 95% confidence. None of the differences between conditions were statistically significant. The linear appearance of the data points in the implicit time plots is due to the temporal resolution of the system (1.04 seconds).

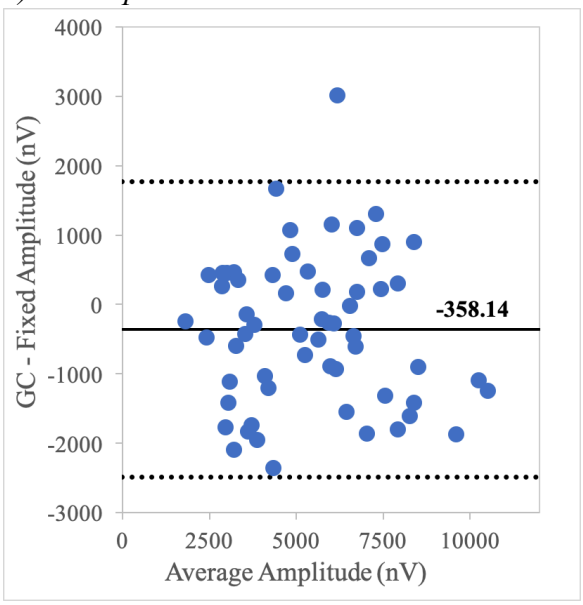
A) N1 Amplitude



B) N1 Implicit Time



*C) P1 Amplitude**



*D) P1 Implicit Time**

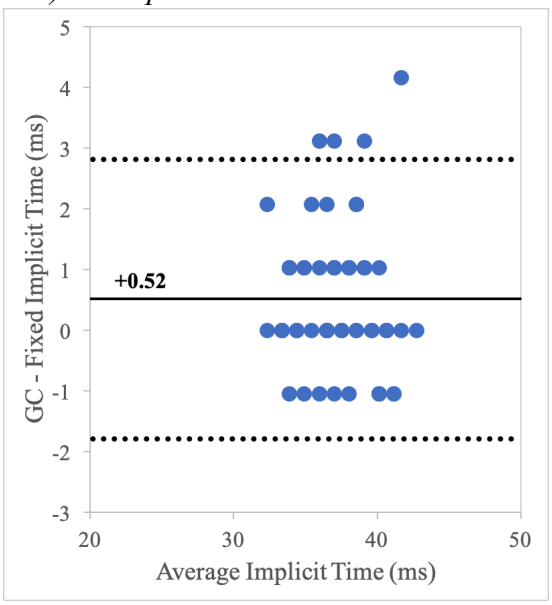


Figure 11) Bland-Altman Plots for Peripheral Stimulus Squares. The solid line represents the average difference between GC and Fixed conditions. The dotted lines represent the upper and lower limit of 95% confidence. Asterisks indicate components with a statistically significant difference between conditions. The linear appearance of the data points in the implicit time plots is due to the temporal resolution of the system (1.04 seconds).

Table 3) Significance testing. The sample size for each data set is the number of paired data points from the GC and Fixed conditions between all subjects. Each significance value is accompanied by the specific test used per the normality testing described in the Methods.

Data set	**Sample size (pairs)**	**Average difference (GC - Fixed) (Mean ± Standard Deviation)**	**Significance test and *p* value (GC vs. Fixed)**
SNR	n = 72	-0.30 ± 2.98	Wilcoxon Signed-Rank test $p = 0.20766$
Eye movements (BCEA)	n = 8	+0.63 ± 2.49 degrees^2	Sign test $p = 0.479$
Eye movements (KDEA)	n = 8	+0.89 ± 2.21 degrees^2	Sign test $p = 1$
N1 Amplitude (all squares)	n = 68	+180.12 ± 938.85 nV	Wilcoxon Signed-Rank test $p = 0.11184$
N1 Implicit Time (all squares)	n = 68	+0.29 ± 1.23 ms	Paired t-test $p = 0.0556$
P1 Amplitude (all squares)*	n = 68	-413.64 ± 1176.04 nV	Paired t-test $p = 0.005$*
P1 Implicit time (all squares)*	n = 68	+0.49 ± 1.13 ms	Paired t-test $p = 0.0007$*
N1 Amplitude (central square)	n = 8	+181.48 ± 1125.07 nV	Paired t-test $p = 0.662$
N1 Implicit Time (central square)	n = 8	+0.13 ± 0.67 ms	Sign test $p = 0.5637$
P1 Amplitude (central square)	n = 8	-829.24 ± 1759.40 nV	Paired t-test $p = 0.224$
P1 Implicit time (central square)	n = 8	+0.26 ± 0.74 ms	Sign test $p = 0.31731$
N1 Amplitude (peripheral squares)	n = 60	+179.94 ± 922.38 nV	Paired t-test $p = 0.1361$
N1 Implicit Time (peripheral squares)	n = 60	+0.31 ± 1.29 ms	Paired t-test $p = 0.0657$
P1 Amplitude (peripheral squares)*	n = 60	-358.14 ± 1084.76 nV	Paired t-test $p = 0.0131$*
P1 Implicit time (peripheral squares)*	n = 60	+0.52 ± 1.17 ms	Paired t-test $p = 0.0011$*

5. DISCUSSION

5.1 SIGNAL-TO-NOISE RATIO

Before using a custom-built system, it is first important to establish the quality of the mfERG results. Qualitatively, the mfERG responses obtained appear similar to the mfERG traces described in previous studies[10, 11]. The purpose of using the SNR was to have a mathematical model in which signal quality could be assessed and unreliable data could be removed. Based on these calculations, only 3% of the signals obtained from the stimulus in all subjects came back lower than the assigned threshold of 2.0. Interestingly, all of those signals were from the same subject, which may speak more to the reliability of the subject rather than the system itself. By comparing the means of the SNR for the GC and Fixed conditions, the lack of a significant difference between the two conditions shows that both recordings were able to produce signals of similar quality, even when the low SNR values were included. This serves as a form of reassurance that the data acquisition using gaze contingency did not introduce excessive noise and that any differences found when comparing the different signal components were not influenced by signal quality.

5.2 EYE MOVEMENTS

When using a gaze contingent display where a visible stimulus follows the subject's gaze, a concern may be that the subject might be further tempted to move their eyes toward the direction of the moving stimulus resulting in a greater area of eye movements when compared to a non-gaze contingent equivalent. However, upon assessing the subjects eye movements using both BCEA and KDEA metrics, there was no significant difference in

fixational eye movements between the GC and Fixed conditions. This indicates that the system likely did not induce additional fixation instability in the GC condition. Using the KDEA, the average calculated area of eye movements was 3.44 degrees^2 in the GC condition and 2.55 degrees^2 in the Fixed condition. For reference, 1mm on the retina corresponds to approximately 3˚visual angle. According to Curcio et al, at 1mm retinal eccentricity the cone density drops one order of magnitude compared to its peak[4]. Because the calculated areas generally surround the central point, the average area of eye movements in this study indicate that the majority of eye movements were within this high density range.

5.3 SIGNAL COMPONENTS

By analyzing the individual signal components, we were able to determine that when all the squares from the stimulus were included, the GC condition had a significantly lower P1 amplitude and significantly longer P1 implicit time compared to the Fixed condition. Furthermore, when separating the stimulus into the central squares and the peripheral squares, the same findings held true for the peripheral squares while no significant differences were observed in the central squares.

It is first important to address that there was a significant difference observed in the P1 values between the two conditions, but not the N1. One explanation for the discrepancy between P1 and N1 amplitudes could be how each component is measured. In a 2002 study by Hood et al, they determined the cellular responses correlating to each portion of the mfERG signal in primates using pharmacologic agents in monkeys and extrapolating the data to a human mfERG recording[13]. *Figure 12* shows two waveforms from their paper with

labeled cellular components. From this, we can presume that the N1 amplitude is made up of cone and OFF-bipolar cell hyperpolarization and the P1 response is made up of ON-bipolar cells' depolarization. However, the N1 response is measured from baseline, while the P1 response is measured from the N1 trough to the P1 peak[2]. Therefore, P1 seems to be more representative of a cumulative cellular response opposed to N1. Because the N1 only accounts for a portion of the total cellular response, this could have made finding any significant differences in the N1 waveform more difficult. Although this theory does not apply to N1 implicit time, in standard ISCEV practice N1 implicit times are not always included[2], which may indicate less diagnostic value than its P1 counterpart.

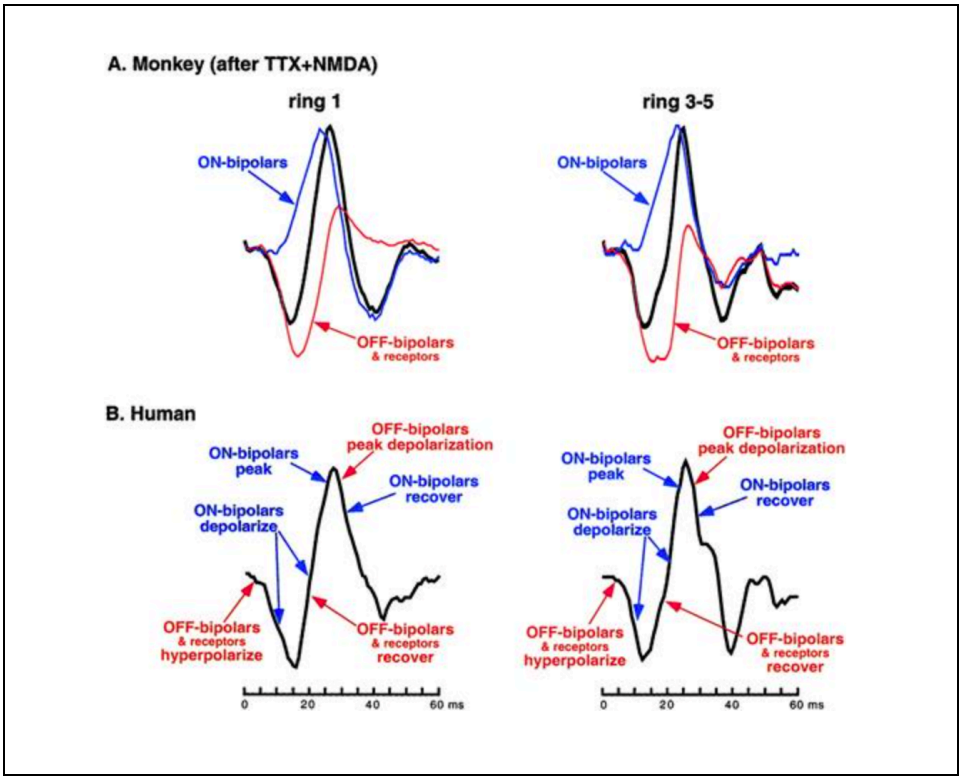


Figure 12) Cellular contributions to an mfERG. This figure adapted from Hood et al's "Retinal origins of the primate multifocal ERG: implications for the human response" shows in panel A a monkey mfERG signal and the cellular contributions determined via pharmacologic agents in both central (left) and peripheral (right) stimulus rings. Panel B shows a human mfERG using the same stimulus and how pharmacologic data was extrapolated and applied to determine what we now know as the accepted human mfERG cellular responses. The human signal also differentiates between central (left) and peripheral (right) stimulus rings.[13]

The reason behind separating the stimulus into central and peripheral squares lies in the distribution of cone and bipolar cell density throughout the retina, as these are the major contributors to the mfERG signal. Cone density is highest in the fovea and decreases towards the periphery. Bipolar cells follow this same distribution. *Figure 13* shows two graphs from a review paper by Grünert and Martin highlighting this change in cone and bipolar cell

distribution as a function of eccentricity throughout a primate retina[36]. In the Fixed condition, the stimulus was able to move across the retina corresponding to each subject's eye movements, causing crossover of high and low density retinal areas. In the GC condition, this was avoided by syncing the stimulus with the subject's fixation and presumably the fovea. If eye movements were large or frequent enough to cause significant crossover, it would be expected that correction with gaze contingency would result in increased central amplitude and decreased peripheral amplitude. However, our results only support the latter. One explanation for this could be the small sample size for the central stimulus squares compared to the peripheral (8 vs. 60), making it difficult to prove significance. The central stimulus of an mfERG is also known to be quite variable between subjects[2], which may influence its reliability in a small sample size. Given these limitations, it is possible that the eye movements displayed by the subjects, although small, were significant enough to cause a difference in amplitude. However, when comparing the average difference in P1 amplitude and the average difference in KDEA for the 8 subjects, there is a poor correlation ($R^2 = .008$). This indicates that the extent of eye movements was not related to the magnitude of difference in P1 amplitude between the two conditions.

It is also important to point out that the average difference in P1 amplitude for the central squares, although not significant, followed a similar trend as the peripheral squares. The average difference in amplitude was negative, meaning the GC condition still had a lower amplitude compared to the Fixed for the central squares. Although the limitations described above could still play a role in these findings, this is the opposite of what we would expect based on retinal anatomy. The significant difference in P1 implicit time is also

difficult to explain in the absence of pathology. We were not able to find any physiological explanation as to why the GC condition would have a longer implicit time. For these two reasons, an alternative scenario explaining the differences in signal components should be considered. It is possible that the gaze contingency itself had an effect on the P1 amplitude and/or implicit time. Instead of relying on an external explanation, the flaw could be within the system. Both of these explanations should be considered in the future studies using this custom-built system.

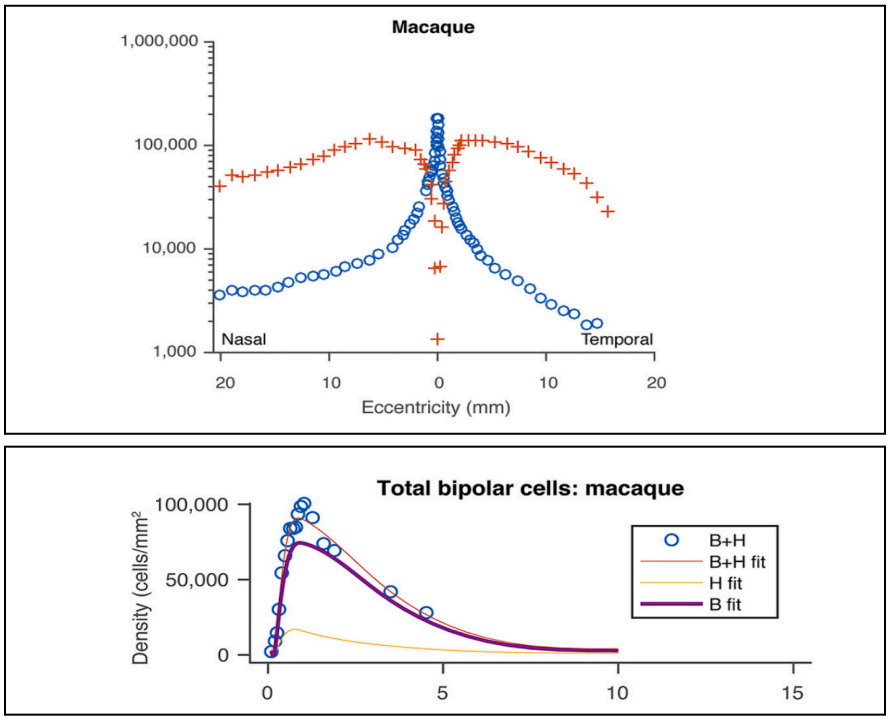


Figure 13) Photoreceptor and bipolar cell density in a primate retina. This figure adapted from Grünert & Martin's "Cell types and cell circuits in human and non-human primate retina" displays cellular distributions of a macaque retina, for which the y-axis shows density (cells/mm^2) as a function of retinal eccentricity (mm) on the x-axis. The upper panel shows the cone (blue) and rod (red) distribution while the purple line in the bottom panel shows the total bipolar cell distribution.[36]

5.4 CORRECTING FOR MULTIPLE COMPARISONS

In the analysis, a *p*-value of less than 0.05 was used across all data sets to determine significance. When assessing the mfERG data, a correction for multiple comparisons should be considered to control for type I error due to the 4 different signal components used. This can be done by applying a Bonferroni correction, where we divide the assigned *p*-value by 4 to account for the different signal components (new *p*-value = 0.0125). In doing so, the P1 amplitude and implicit time when including all stimulus squares holds its significance as well as the P1 implicit time for the peripheral squares. However, it causes the P1 amplitude for the peripheral squares to fall just outside of significance ($p = 0.0131$). In the discussion above addressing the different signal components, all 4 of the initial values were addressed as being significant. This was because the Bonferroni correction tends to be a more conservative method. Additionally, all significant values were well below the initial $p = 0.05$.

5.5 STUDY LIMITATIONS

One limitation of the study is the stimulus itself. When comparing the stimulus used in this study (*Figure 4*) to a standard hexagonal mfERG stimulus (*Figure 1)*, there are some major differences, including the number and size of the hexagons as well as a lack of scaling with eccentricity. The custom-built system used in this study is still in early stages of development and the aim of the study was geared towards proof of concept instead of real-world applications, which is why this more simplistic design was created. However, it is important to acknowledge that most of the background research and comparisons made in the study reference a standard mfERG stimulus.

Another major limitation in the study was the number of subjects. The original power analysis required 10 subjects for a power of 0.9. Testing was attempted in 11 subjects, but 3 subjects were ultimately excluded causing our sample size to fall below this threshold. As mentioned in the methods, at the time the present study was being conducted, another stimulus was simultaneously being tested with our same custom-built system and protocol. This additional stimulus was designed to more closely mimic a standard mfERG stimulus. Because of this, the decision was made to divide the total number of interested participants between the two stimuli. We anticipated being able to use both sets of data, but due to technical limitations only the one was included.

Additionally, it should be mentioned that the subjects' fixation was not explicitly screened as an inclusion criterion for the study. Subjects were assumed to have normal fixation based on their normal vision and the absence of confounding variables, but this may not guarantee accurate fixation. It was qualitatively observed that many subjects had difficulty with attention throughout testing, likely due to the length of the experiment. An interesting addition to the study could have been a full binocular vision assessment with measures of eye movements. This may have provided useful information about subject behavior and could have been used as an additional criterion to help predict good fixation.

5.6 FUTURE APPLICATIONS

After testing the custom-built system on subjects with normal vision and determining that the SNR and fixational eye movements are consistent between the GC and Fixed conditions, the proposed next step is to use the system in subjects with fixation instability.

Before a system like this can be applied clinically, it is important to ensure that in the presence of larger eye movements the system is still able to produce a viable signal both with and without gaze contingency. Although mfERGs are most commonly used in those with retinal pathologies, disease processes like ARMD could make analyzing the effect of eye movements difficult due to its variable nature. Instead, it would be best to test subjects with poor fixation in the absence of progressive retinal pathology. One group of people that may fit this criterion are persons with albinism. This population is of interest because of their commonly associated nystagmus and stable retinal findings, specifically foveal hypoplasia[37]. By using these subjects, you nearly guarantee fixation instability while assuring stable retinal findings for comparison.

6. CONCLUSIONS

When assessing the SNR and eye movement data, the lack of significance between the two conditions indicates that the addition of gaze contingency to the custom-built system does not significantly affect signal quality nor the extent of eye movements in subjects with presumed normal fixation. These findings support the continuation of research utilizing this system, with the goal of eventually testing subjects with fixation instability. However, the lack of power in this study should be considered when interpreting these results. Upon comparing the signal components between the two conditions, it was determined that there was a small but significant difference in P1 amplitude and implicit time when assessing the data that included all stimulus squares and the peripheral stimulus squares. More specifically, the GC condition had a significantly lower P1 amplitude and significantly longer P1 implicit time when compared to the Fixed condition. The difference in P1 amplitude can be anatomically explained by an increase in spatial specificity in the GC condition leading to less crossover between high and low response areas on the retina. It is also possible that the differences observed are instead a consequence of the gaze contingency itself in the custom-built system. However, given the limitations of the study, we cannot be certain as to which is more likely. Moving forward, both of these explanations should be considered.

7. BIBLIOGRAPHY

1. Gupta, M. P., Herzlich, A. A., Sauer, T., & Chan, C. C. (2016). Retinal anatomy and pathology. *Retinal Pharmacotherapeutics, 55, 7-17.*
2. Hildebrand, G. D., & Fielder, A. R. (2011). Anatomy and physiology of the retina. *Pediatric retina, 39-65.*
3. Provis, J. M., Penfold, P. L., Cornish, E. E., Sandercoe, T. M., & Madigan, M. C. (2005). Anatomy and development of the macula: specialization and the vulnerability to macular degeneration. *Clinical and Experimental Optometry, 88(5), 269–281. https://doi.org/10.1111/j.1444-0938.2005.tb06711.x*
4. Curcio, C. A., Sloan, K. R., Kalina, R. E., & Hendrickson, A. E. (1990). Human photoreceptor topography. *Journal of comparative neurology, 292(4), 497-523.*
5. Keane, P. A., & Sadda, S. R. (2014). Retinal imaging in the twenty-first century: state of the art and future directions. *Ophthalmology, 121(12), 2489-2500.*
6. Arden, G. B., & Constable, P. A. (2006). The electro-oculogram. *Progress in retinal and eye research, 25(2), 207-248.*
7. Bhatt, Y., Hunt, D. M., & Carvalho, L. S. (2023). The origins of the full-field flash electroretinogram b-wave. *Frontiers in Molecular Neuroscience, 16.*
8. Robson, A. G., Frishman, L. J., Grigg, J., Hamilton, R., Jeffrey, B. G., Kondo, M., ... & McCulloch, D. L. (2022). ISCEV Standard for full-field clinical electroretinography (2022 update). *Documenta Ophthalmologica, 144(3), 165-177.*

9. Thompson, D. A., Bach, M., McAnany, J. J., Šuštar Habjan, M., Viswanathan, S., & Robson, A. G. (2024). ISCEV standard for clinical pattern electroretinography (2024 update). *Documenta Ophthalmologica, 1-11.*

10. Sutter, E. E., & Tran, D. (1992). The field topography of ERG components in man—I. The photopic luminance response. *Vision research, 32(3), 433-446.*

11. Hoffmann, M. B., Bach, M., Kondo, M., Li, S., Walker, S., Holopigian, K., ... & Robson, A. G. (2021). ISCEV standard for clinical multifocal electroretinography (mfERG)(2021 update). *Documenta Ophthalmologica, 142, 5-16.*

12. Müller, P. L., & Meigen, T. (2016). M-sequences in ophthalmic electrophysiology. *Journal of Vision, 16(1), 15-15.*

13. Hood, D. C., Frishman, L. J., Saszik, S., & Viswanathan, S. (2002). Retinal origins of the primate multifocal ERG: implications for the human response. *Investigative ophthalmology & visual science, 43(5), 1673-1685.*

14. Hood, D. C., Odel, J. G., Chen, C. S., & Winn, B. J. (2003). The multifocal electroretinogram. *Journal of Neuro-Ophthalmology, 23(3), 225-235.*

15. Lai, T. Y., Chan, W. M., Lai, R. Y., Ngai, J. W., Li, H., & Lam, D. S. (2007). The clinical applications of multifocal electroretinography: a systematic review. *Survey of ophthalmology, 52(1), 61-96.*

16. Renner, A. B., Kellner, U., Tillack, H., Kraus, H., & Foerster, M. H. (2005). Recording of both VEP and multifocal ERG for evaluation of unexplained visual loss: Electrophysiology in unexplained visual loss. *Documenta ophthalmologica, 111, 149-157.*

17. Ambati, J., & Fowler, B. J. (2012). Mechanisms of age-related macular degeneration. *Neuron, 75(1), 26-39.*

18. Mitchell, P., Liew, G., Gopinath, B., & Wong, T. Y. (2018). Age-related macular degeneration. *The Lancet, 392(10153), 1147-1159.*

19. Yavas, G. F., Küsbeci, T., & Inan, Ü. Ü. (2014). Multifocal electroretinography in subjects with age-related macular degeneration. *Documenta Ophthalmologica, 129, 167-175.*

20. Yang, S., Zuo, C., Xiao, H., Mi, L., Luo, G., Xu, X., & Liu, X. (2016). Photoreceptor dysfunction in early and intermediate age-related macular degeneration assessed with mfERG and spectral domain OCT. *Documenta Ophthalmologica, 132, 17-26.*

21. Kretschmann, U., Seeliger, M. W., Ruether, K., Usui, T., Apfelstedt-Sylla, E., & Zrenner, E. (1998). Multifocal electroretinography in patients with Stargardt's macular dystrophy. *British journal of ophthalmology, 82(3), 267-275.*

22. Jarc-Vidmar, M., Perovšek, D., Glavač, D., Brecelj, J., Hawlina, M., & Stirn-Kranjc, B. (2012). Morphology and function of the retina in children and young adults with stargardt dystrophy.

23. Gerth, C., Wright, T., Héon, E., & Westall, C. A. (2007). Assessment of central retinal function in patients with advanced retinitis pigmentosa. *Investigative ophthalmology & visual science, 48(3), 1312-1318.*

24. Hood, D. C. (2000). Assessing retinal function with the multifocal technique. *Progress in retinal and eye research, 19(5), 607-646.*

25. Chu, P. H., Chan, H. H., & Leat, S. J. (2006). Effects of unsteady fixation on multifocal electroretinogram (mfERG). *Graefe's Archive for Clinical and Experimental Ophthalmology, 244, 1273-1282.*

26. Pedersen, K. B., Sjølie, A. K., Vestergaard, A. H., Andréasson, S., & Møller, F. (2016). Fixation stability and implication for multifocal electroretinography in patients with neovascular age-related macular degeneration after anti-VEGF treatment. *Graefe's Archive for Clinical and Experimental Ophthalmology, 254, 1897-1908.*

27. Tosha, C., Gorin, M. B., & Nusinowitz, S. (2010). Test-retest reliability and inter-ocular symmetry of multi-focal electroretinography in Stargardt disease. *Current Eye Research, 35(1), 63-72.*

28. Alexander, R. G., & Martinez-Conde, S. (2019). Fixational eye movements. *Eye movement research: An introduction to its scientific foundations and applications, 73-115..*

29. Martinez-Conde, S., Macknik, S. L., & Hubel, D. H. (2004). The role of fixational eye movements in visual perception. *Nature reviews neuroscience, 5(3), 229-240.*

30. Kumar, G., & Chung, S. T. (2014). Characteristics of fixational eye movements in people with macular disease. *Investigative ophthalmology & visual science, 55(8), 5125-5133.*

31. Loschky, L. C., & McConkie, G. W. (2002). Investigating spatial vision and dynamic attentional selection using a gaze-contingent multiresolutional display. *Journal of Experimental Psychology: Applied, 8(2), 99.*

32. Ganesan, S., Melnik, N., Azanon, E., & Pollmann, S. (2023). A gaze-contingent saccadic re-referencing training with simulated central vision loss. *Journal of Vision, 23(1), 13-13.*

33. Dorr, M., & Bex, P. J. (2011, February). A gaze-contingent display to study contrast sensitivity under natural viewing conditions. *In Human Vision and Electronic Imaging XVI (Vol. 7865, pp. 324-331). SPIE.*

34. Harrison, W. W., Bearse, M. A., Ng, J. S., Barez, S., Schneck, M. E., & Adams, A. J. (2009). Reproducibility of the mfERG between instruments. *Documenta ophthalmologica, 119, 67-78.*

35. Zhang, X., Hood, D. C., Chen, C. S., & Hong, J. E. (2002). A signal-to-noise analysis of multifocal VEP responses: an objective definition for poor records. *Documenta Ophthalmologica, 104, 287-302.*

36. Grünert, U., & Martin, P. R. (2020). Cell types and cell circuits in human and non-human primate retina. *Progress in retinal and eye research, 78, 100844.*

37. Summers, C. G. (2009). Albinism: classification, clinical characteristics, and recent findings. *Optometry and vision Science, 86(6), 659-662.*